PHOTOSYNTHETICA
International Journal for Photosynthesis Research

DOI 10.32615/ps.2026.004 PHOTOSYNTHETICA 64 (1): 43-51, 2026

Elucidating copper ion interactions with carbonic anhydrase: insights from fluorescence quenching and thermodynamic analysis

M.S. SHABANOVA[*], I.M. HUSEYNOVA[*], S.K. ZHARMUKHAMEDOV[**,+], and S.I. ALLAKHVERDIEV[**,***,#,##,+]

*Institute of Molecular Biology, Ministry of Science and Education of the Republic of Azerbaijan, 11 Izzat Nabiyev Str., AZ1073, Baku, Azerbaijan**
*Institute of Basic Biological Problems, Russian Academy of Sciences, Institutskaya Street 2, 142290 Pushchino, Moscow Region, Russia***
*Department of Plant Physiology, Faculty of Biology, M.V. Lomonosov Moscow State University, Leninskie Gory 1-12, 119991 Moscow, Russia****
K.A. Timiryazev Institute of Plant Physiology, Russian Academy of Sciences, Botanicheskaya Street 35, 127276 Moscow, Russia#
Faculty of Engineering and Natural Sciences, Bahcesehir University, Istanbul, Turkey##

Abstract

Plant carbonic anhydrases (CAs) are essential metalloenzymes catalyzing reversible hydration of CO_2 to HCO_3^-, thereby optimizing photosynthetic efficiency and carbon fixation in plants. They facilitate CO_2 delivery to Rubisco, enhance carbon assimilation, and play a role in plant responses to stresses (such as drought, high salinity) by modulating stomatal conductance and internal CO_2 concentrations. Despite the well-established physiological importance of plant CAs, the influence of metal ions, particularly copper (Cu^{2+}), on their structure and activity remains inadequately understood. Here, bCA II is used as a well-characterized model enzyme to investigate enzyme–metal interactions. We employed intrinsic tryptophan and tyrosine fluorescence quenching to elucidate the binding mechanism of Cu^{2+} with bCA II. Our results demonstrate static quenching, indicative of ground-state complex formation, with binding parameters assessed at 288 K and 298 K [Kb = (2.64 ± 0.15 and 1.68 ± 0.54) × 10^3, M^{-1}, n ≈ 1] and negative ΔG°, ΔH°, ΔS°.

Keywords: bovine CA II; copper ions; enzyme–metal interaction; fluorescence quenching; plant carbonic anhydrase; thermodynamics.

Introduction

Carbonic anhydrases (CAs) constitute a superfamily of among the most ancient and evolutionarily conserved metalloenzymes, ubiquitously distributed across all domains of life – from bacteria to humans – that catalyze the fundamental reaction of reversible carbon dioxide hydration to bicarbonate and protons (Supuran 2008,

Highlights

- The bCA II was used as a model to investigate enzyme–Cu^{2+} interactions
- Enzyme fluorescence quenching clarifies the binding mechanism of Cu^{2+} with bCA II
- Static quenching indicates ground-state complex formation at 288 K, 298 K

Received 12 February 2026
Accepted 2 March 2026
Published online 10 March 2026

[+]Corresponding authors
e-mail: watcher01@rambler.ru (SKZ)
suleyman.allakhverdiev@gmail.com (SIA)

Abbreviations: bCA II – bovine carbonic anhydrase II; F – fluorescence; K_{SV} – Stern–Volmer constant; K_b – association constant; kq – bimolecular quenching rate constants.
Acknowledgements: This work was supported by a grant from the Russian Science Foundation (No. 24-14-00033). Additionally, Figs. 3 and 4 were funded under the state contract from the Ministry of Science and Higher Education of the Russian Federation (themes No. 125051305928-7 and 126012015840-2). Work was done with equipment of shared Core Facilities of the Pushchino Scientific Center for Biological Research (http://www.ckp-rf.ru/ckp/670266/).
Conflict of interest: The authors declare that they have no conflict of interest.

2016a). To date, the carbonic anhydrase superfamily is classified into eight evolutionarily independent families (α, β, γ, δ, ζ, η, θ, and ι) (Nocentini *et al.* 2021, Fedai *et al.* 2025), which arose through convergent evolution and lack primary sequence homology. Owing to their exceptionally high catalytic efficiency, carbonic anhydrases play critical roles in ensuring rapid inorganic carbon flux and regulation of intra- and extracellular pH homeostasis, facilitating CO_2 transport, and modulating electrolyte secretion across diverse tissues and organisms; they participate in key physiological processes including respiration, electrolyte secretion, gluconeogenesis, lipogenesis, bone formation, and production of bodily fluids (cerebrospinal, gastric, and saliva) (Frost 2014, Kupriyanova *et al.* 2017, Supuran 2023).

In photosynthetic cells, carbonic anhydrases perform a catalytic function by accelerating CO_2/HCO_3^- interconversion, enabling carbon-concentrating mechanisms (CCM), regulating intracellular and intraorganellar pH, and facilitating inorganic carbon transport across membranes. Furthermore, these enzymes contribute to stomatal regulation, modulate stress-responsive signaling pathways, protect against oxidative damage, support adaptation to abiotic stresses, participate in chloroplast development, and supply bicarbonate for biosynthetic reactions (Tiwari *et al.* 2005, Rudenko *et al.* 2015, Kupriyanova *et al.* 2017).

Among the numerous carbonic anhydrase isoforms, bCA II is the most extensively studied. It is one of the most catalytically efficient and evolutionarily conserved enzymes, exhibiting high conformational stability, structural accessibility, a well-characterized active site, straightforward purification, and commercial availability. bCA II displays exceptional catalytic efficiency, with a catalytic rate constant for CO_2 hydration of 1.14×10^8 M^{-1} s^{-1} – approaching the diffusion limit (Phan *et al.* 2015). The three-dimensional structure of bCA II was determined by X-ray crystallography, and the architecture of its active site – featuring a Zn^{2+} ion coordinated by three histidine residues and a water/hydroxide ligand – has been extensively refined (Saito *et al.* 2004). These attributes establish bCA II as a universal 'gold standard', 'model system' (Saito *et al.* 2004, Wei *et al.* 2006, Benlloch *et al.* 2015, Phan *et al.* 2015, Lee *et al.* 2018) and the 'workhorse' (Krishnamurthy *et al.* 2008) for studying carbonic anhydrases and any systems exhibiting carbonic anhydrase-like activity. It is routinely used to evaluate and compare catalytic activity, including activity detected in non-canonical systems – such as the extrinsic subunits of PSII (PsbO, PsbP, PsbQ) and even the PSII core complex depleted of these (Shitov *et al.* 2009, 2025). bCA II was used to validate novel methods for estimating carbonic anhydrase activity (Kim and Jo 2022), for the comparative assessment of PSII-associated CAH3 activity in *Chlamydomonas reinhardtii* (Shutova *et al.* 2008), for evaluating PSII-associated carbonic anhydrase activity (McConnell *et al.* 2007), and for characterizing mouse carbonic anhydrase VII expressed in *E. coli* (Lakkis *et al.* 1996). bCA II is widely used as a model carbonic anhydrase in numerous studies: for analyzing the effects of surface charge on denaturation (Gitlin *et al.* 2006); for studying pretransition phenomena and progressive softening (Afrin *et al.* 2005), the molten-globule state (Rajaraman *et al.* 1996), and temperature effects (Sarraf *et al.* 2004); for designing novel approaches to enzyme-induced biomimetic CO_2 sequestration (Asadi *et al.* 2019, Tobolovskaya *et al.* 2023, Mourad *et al.* 2024, Abdulmajeed *et al.* 2025), and for analyzing the effects of novel inhibitors, metals, and organometallic complexes on CA activity (Karacan *et al.* 2014, 2016; Kose *et al.* 2016; Rodionova *et al.* 2017).

Copper – in both ionic form (Cu^{2+}) and as copper–organic complexes – is known to inhibit the photochemical activity of PSII (Burda *et al.* 2002, 2003, 2006; Yruela 2005, Rodionova *et al.* 2017, Zharmukhamedov *et al.* 2022, 2023). Copper ions may also inhibit various carbonic anhydrases. The interaction parameters of Cu^{2+} with CAs are primarily determined from measurements of its inhibitory effect on catalytic activity, which is typically quantified by *p*-nitrophenyl acetate hydrolysis (an esterase activity assay) or, less commonly, by CO_2 hydration. In contrast, studies using other analytical methods, particularly intrinsic fluorescence quenching of enzymes, are comparatively scarce. In one of the main studies using this method, it was shown that a single Cu^{2+} concentration ($2–5 \times 10^{-4}$ M) added to apo-bCA II to form the Cu-bCA II quenched the enzyme's fluorescence to 40% of its initial value, suggesting Cu^{2+}-induced conformational changes (Finazzi Agrò *et al.* 1974). The literature lacks detailed data on the dependence of intrinsic fluorescence quenching magnitude in bCA II (or other CAs), on parameters characterizing the quenching mechanism, and on thermodynamic parameters describing the nature of interaction forces between Cu^{2+} and CAs – particularly as a function of temperature. In our previous studies, we showed that the Cu^{2+}-based organometallic complex $[CuL_2]Br_2$ not only inhibits photoinduced oxygen evolution and electron transport in PSII (Zharmukhamedov *et al.* 2022, 2023), but also possesses potent inhibitory activity against carbonic anhydrase (CA). It effectively suppresses hydration reactions catalyzed by both the CA-like activity of PSII and bCA II, used as a model enzyme for comparison (Rodionova *et al.* 2017). These results highlight the multitarget impact of copper ions and Cu^{2+}-based complexes on photosynthesis and CA activity, emphasizing that inhibition of CA activity is one of the key factors in modulating plant responses to abiotic stresses.

In this work, we performed a detailed analysis of the kinetic and thermodynamic parameters, as well as the nature of the binding forces, for the interaction between copper ions (Cu^{2+}) – as part of our organometallic complexes – and bCA II, using the intrinsic fluorescence quenching method. We anticipate that the obtained data will provide deeper insight into the inhibitory mechanisms of Cu^{2+} ions and copper-based organometallic complexes toward both PSII (its photochemical and CA-like activities) and carbonic anhydrases, including bCA II.

Materials and methods

Materials: Native carbonic anhydrase II from bovine erythrocytes lyophilized powder (Product No. C3934,

Sigma-Aldrich) and all other chemicals were purchased from *Sigma-Aldrich* (St. Louis, MO, USA). According to the manufacturer's specifications, the enzyme exhibited a specific activity of ≥ 2,000 Wilbur–Anderson units per mg protein. Ultrapure water (resistivity ≥ 18.2 MΩ cm at 25°C), obtained from a *Milli-Q*® purification system (*Merck Millipore*, Burlington, MA, USA), was used for the preparation of all aqueous solutions as well as for rinsing cuvettes and all solution containers.

Steady-state fluorescence studies: The source of fluorescence in carbonic anhydrases is intrinsic fluorescence, primarily from the aromatic amino acid residues, with tryptophan (Trp) being the dominant contributor. Tryptophan residues exhibit strong fluorescence when excited at ~280 nm, with emission maxima typically around 330–350 nm depending on their microenvironment (buried *vs*. exposed). Tyrosine (Tyr) can also fluoresce (excitation ~275 nm, emission ~303 nm). But its quantum yield is much lower (~0.14 *vs*. ~0.20 for Trp), and energy transfer from Tyr to Trp often occurs, reducing its observable contribution. Phenylalanine has negligible fluorescence in proteins under standard conditions. This is well-established in biophysical studies of carbonic anhydrase, where Trp fluorescence is widely used to monitor conformational changes, ligand binding, unfolding, and pressure effects (Finazzi Agrò *et al.* 1974, Stein and Henkens 1978, Nemtseva *et al.* 2017). For bCA II, the mature protein sequence consists of 259–260 amino acids (depending on whether the initiating methionine is included in numbering; most structures use 260 residues including Met1). It contains: 7 tryptophan (Trp, W) residues and 8 tyrosine (Tyr, Y) residues. These numbers are confirmed across multiple sources, including direct sequence data and studies that map Trp accessibility or fluorescence contributions in bCA II (*e.g*., chemical modification and spectral decomposition studies explicitly refer to its seven tryptophan residues). The Trp positions in the standard numbering (including Met1) are typically W5, W16, W97, W123, W191, W208, W244 (or slight shifts depending on alignment, but consistently 7 total) (Sciaky *et al.* 1976, Ladner *et al.* 2007).

As a fluorescence quencher for bCA II, a $CuCl_2$ solution prepared in 50 mM Tris buffer (pH 7.5) was employed.

Fluorescence quenching experiments were carried out using a *Varian Cary Eclipse* fluorescence spectrophotometer (*Agilent Technologies*, Santa Clara, USA). The temperature inside the cuvette was adjusted and held constant at the required value using a *Single-Cell Peltier Accessory* for the *Cary Eclipse* (*Agilent Technologies*) connected to a water-bath thermostat. All experiments were performed at three temperatures: 288 K, 298 K, and 308 K. The temperature was maintained during measurements with an accuracy of ± 0.1°C. Fluorescence emission spectra were recorded with an excitation wavelength of 280 nm and an emission range of 300–450 nm, using 10-nm slit widths for both excitation and emission. All sample preparations were conducted under dim illumination to prevent light-induced generation of reactive oxygen species – particularly in the presence of Cu^{2+} – which could otherwise affect enzyme integrity. Following all required additions, samples were allowed to equilibrate in the cuvette in the dark for 3 min before measurement. All fluorescence intensities were corrected for the inner filter effect (Lakowicz 2006).

Calculation of quenching parameters and statistics: All fluorescence measurements were performed as independent biological replicates (n = 3 per condition), with emission spectra representing averages of three to five replicates as indicated. Descriptive statistics included mean fluorescence intensity (F) with associated standard deviation (SD) and standard error of the mean (SE) calculated as SD/√n. Stern–Volmer analysis employed linear regression of F_0/F *vs.* $[Cu^{2+}]$ according to $F_0/F = 1 + K_{SV}[Cu^{2+}]$, with regression parameters (intercept, slope ± standard error of the fit) and correlation coefficients (R^2) determined using least-squares minimization. The Stern–Volmer constant (K_{SV}) was derived directly from the slope, and the bimolecular quenching rate constant (kq) was calculated as $kq = K_{SV}/\tau_0$ assuming a tryptophan fluorescence lifetime $\tau_0 = 10^{-8}$ s, with error propagation maintaining relative uncertainty. Modified Stern–Volmer (double-logarithmic) analysis utilized linear regression of $\log_{10}[(F_0–F)/F]$ *vs*. $\log_{10}[Cu^{2+}]$ to determine binding stoichiometry (n, from slope) and association constant (K_b, from intercept) with 95% confidence intervals (CI) calculated from regression standard errors using *Student*'s *t*-distribution (degrees of freedom df = N – 2, where N = 5 Cu^{2+} concentrations). Statistical significance of temperature-dependent differences in binding parameters was assessed by a two-tailed *Student*'s *t*-test ($\alpha = 0.05$). Thermodynamic parameters were derived from van't Hoff analysis *via* linear regression of $\ln K_b$ *vs*. 1/T; ΔH° and ΔS° were obtained from the slope ($-\Delta H°/R$) and intercept ($\Delta S°/R$) with 95% CI, while ΔG° was calculated directly at each temperature using $\Delta G° = -RT \ln K_b$ with error propagation from K_b confidence intervals. Non-linearity in the van't Hoff plot prompted interval-specific thermodynamic analysis (288–298 K and 298–308 K) to account for potential heat capacity changes ($\Delta Cp \neq 0$). All statistical analyses and graphical fittings were performed using *OriginPro 2023* (*OriginLab Corporation*, Northampton, MA, USA) with significance defined as $p<0.05$.

Results and discussion

Cu^{2+}-induced quenching of bCA II inherent fluorescence: Fig. 1 shows fluorescence emission spectra of bCA II (1 μM) recorded at 288 K, 298 K, and 308 K in the absence and presence of increasing Cu^{2+} concentrations (0–1.00 mM). Under all conditions, the emission maximum remained fixed at 343 nm. It did not shift with increasing $[Cu^{2+}]$, indicating the absence of significant conformational rearrangements in the protein's tertiary structure within the studied concentration range. A dose-dependent quenching of fluorescence was observed, with intensity progressively decreasing as Cu^{2+} concentration increased. At 288 K, fluorescence intensity ranged from

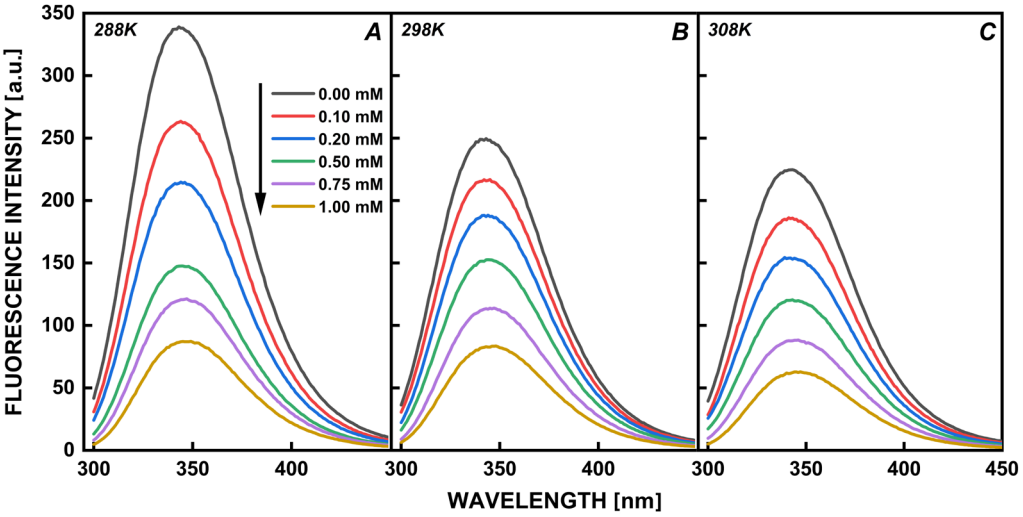

Fig. 1. Fluorescence emission spectra of bCA II (1 μM) in the absence and presence of increasing Cu^{2+} concentrations (0, 10, 25, 50, 75, 100 μM) at 288 K (*A*), 298 K (*B*), and 308 K (*C*) in 50 mM Tris-buffer, pH 7.5. The excitation wavelength was 280 nm; emission was recorded from 300 to 450 nm using 10-nm slit widths for both excitation and emission. The arrow indicates the direction of decreasing fluorescence intensity with increasing Cu^{2+} concentration. Each spectrum represents the average of three to five independent biological replicates.

a maximum of 339.03 a.u. (without additive) to a minimum of 86.48 a.u. (1.00 mM Cu^{2+}); at 298 K from 249.52 to 82.94 a.u.; and at 308 K from 224.66 to 62.24 a.u. The most pronounced quenching occurred at 288 K, where the fluorescence intensity decreased by approximately 74.5% at 1.00 mM Cu^{2+}, compared to reductions of ~66.8% at 298 K and ~72.3% at 308 K. All spectra represent averages of three independent biological replicates, confirming the reproducibility of the observed quenching effect.

Mechanism for Cu^{2+}-induced fluorescence quenching of bCA II: To determine the quenching mechanism – static, dynamic (collisional), or mixed – a Stern–Volmer plot of the intensity ratio (F_0/F) *vs*. [Cu^{2+}] must be constructed, followed by calculation of the Stern–Volmer constant (K_{SV}) and the quenching rate constant (kq) (Lakowicz 2006, Wani *et al.* 2017, Sargolzaei *et al.* 2024). Stern–Volmer analysis of the fluorescence quenching data revealed linear relationships between F_0/F and [Cu^{2+}] at all three temperatures (Fig. 2), with correlation coefficients (R^2) ranging from 0.958 to 0.985 (Table 1), confirming adherence to the Stern–Volmer equation $F_0/F = 1 + K_{SV} \times [Cu^{2+}]$. At 288 K, the Stern–Volmer constant was $K_{SV} = (2.75 \pm 0.17) \times 10^3$ M^{-1}. At 298 K, K_{SV} decreased to $(1.88 \pm 0.19) \times 10^3$ M^{-1}, and at 308 K, K_{SV} was $(2.44 \pm 0.24) \times 10^3$ M^{-1}. The overall reduction in K_{SV} from 288 K to 298 K – despite a slight increase at 308 K – aligns with the characteristic temperature dependence of static quenching, where quenching efficiency diminishes with rising temperature due to destabilization of the ground-state complex. This interpretation is further supported by the calculated bimolecular quenching rate constants (kq), which exceeded the diffusion-controlled limit (~10^{10} M^{-1} s^{-1}) at all temperatures: $(2.75 \pm 0.17) \times 10^{11}$ M^{-1} s^{-1} (288 K), $(1.88 \pm 0.19) \times 10^{11}$ M^{-1} s^{-1} (298 K),

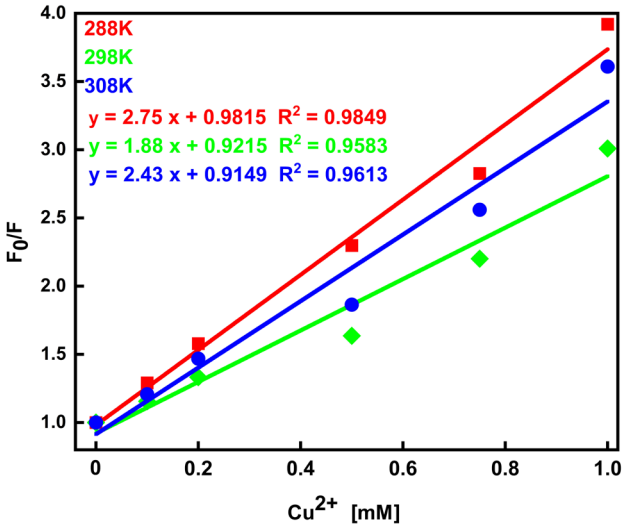

Fig. 2. Stern–Volmer plots (F_0/F *vs*. [Cu^{2+}]) for bCA II (1 μM) in 50 mM Tris buffer, pH 7.5, at 288 K (*red line and equation*), 298 K (*green line and equation*), and 308 K (*blue line and equation*). The linear regression fits (*solid lines*) correspond to the Stern–Volmer equation $F_0/F = 1 + K_{SV} \times [Cu^{2+}]$. The decrease in Stern–Volmer constants (K_{SV}) with increasing temperature indicates static quenching. Correlation coefficients (R^2) and K_{SV} values (in M^{-1}) are shown on the plots and listed in Table 1.

and $(2.44 \pm 0.24) \times 10^{11}$ M^{-1} s^{-1} (308 K). Such anomalously high kq values are physically implausible for a dynamic (collisional) process and instead indicate formation of a non-fluorescent ground-state complex between Cu^{2+} and bCA II. Consequently, the quenching mechanism is unequivocally static. Given that static quenching arises from specific binding interactions in the ground state, the Stern–Volmer constant K_{SV} directly corresponds to the association constant (K_b) for the Cu^{2+}–bCA II complex.

Table 1. Stern–Volmer parameters for Cu^{2+}-induced quenching of bCA II fluorescence at three temperatures. Linear regression of F_0/F *vs*. $[Cu^{2+}]$ yielded intercepts, slopes (equal to K_{SV}), correlation coefficients (R^2), Stern–Volmer constants (K_{SV}), and bimolecular quenching rate constants (kq, calculated assuming $\tau_0 = 10^{-8}$ s for tryptophan fluorescence lifetime). Values represent mean ± standard error of the regression fit. All K_{SV} values are expressed in M^{-1}; kq values in M^{-1} s^{-1}.

pH	T [K]	Intercept	Slope	R^2	K_{SV}, × 10^3, [M^{-1}]	Kq, × 10^{11}, [M^{-1} s^{-1}]
7.5	288	0.98157 ± 0.09473	2.75485 ± 0.17003	0.98499	2.75 ± 0.17	2.75 ± 0.17
	298	0.92158 ± 0.10957	1.88453 ± 0.19667	0.95826	1.88 ± 0.19	1.88 ± 0.19
	308	0.91494 ± 0.13634	2.43936 ± 0.24471	0.96130	2.44 ± 0.24	2.44 ± 0.24

Table 2. Binding parameters for Cu^{2+} interaction with bCA II derived from modified Stern–Volmer (double-logarithmic) analysis at 288 K, 298 K, and 308 K (50 mM Tris buffer, pH 7.5). Values are expressed as mean ± 95% confidence interval (CI). Each plotted data point (N = 5 Cu^{2+} concentrations) represents the mean of ≥5 independent fluorescence measurements per concentration. 95% CIs for n and Kb were calculated from regression standard errors using *Student*'s *t*-distribution (df = N – 2). Differences between temperatures were considered statistically significant at $p<0.05$ (two-tailed *Student*'s *t*-test). Each value of F (fluorescence intensity) at a given $[Cu^{2+}]$ represents the arithmetic mean of ≥ 5 independent replicate measurements (technical replicates). The five concentrations used for regression were selected to span the linear region of the double-logarithmic plot (typically 0–100 µM Cu^{2+}). 95% confidence intervals for n (slope) and $\log_{10}$Kb (intercept) were calculated as CI = parameter ± tα/2, df × SE, where t0.025,3 = 3.182 (*Student*'s *t*-coefficient for df = N – 2 = 3 at α = 0.05), and SE is the standard error from linear regression. Statistical comparison of K_b values between temperatures was performed using an unpaired two-tailed *Student*'s *t*-test; $p<0.05$ was considered significant.

pH	T [K]	Intercept	Slope	R^2	Kb, × 10^3, [M^{-1}]	n
7.5	288	0.42104 ± 0.02496	0.95949 ± 0.04419	0.99368	2.64 ± 0.15	0.96 ± 0.04 ≈ 1
	298	0.22412 ± 0.05385	1.04408 ± 0.09534	0.97559	1.68 ± 0.54	1.04 ± 0.10 ≈ 1
	308	0.34268 ± 0.05170	1.02499 ± 0.09155	0.97663	2.20 ± 0.26	1.03 ± 0.09 ≈ 1

This equivalence justifies the progression to quantitative determination of the binding constant and stoichiometry using modified Stern–Volmer (double-logarithmic) analysis or Scatchard plots to elucidate the molecular details of Cu^{2+} interaction with the enzyme.

Quantitative characterization of Cu^{2+} binding to bCA II: stoichiometry and temperature-dependent association constant: To quantitatively characterize the interaction of Cu^{2+} with bCA II, a modified Stern–Volmer analysis in double-logarithmic coordinates was performed (Fig. 3) (Lakowicz 2006, Wani *et al.* 2017, Sargolzaei *et al.* 2024). The dependencies of $\log_{10}[(F_0 – F)/F]$ on $\log_{10}[Cu^{2+}]$ were linear at all temperatures (Table 2), confirming the applicability of the equation $\log_{10}[(F_0 – F)/F] = \log_{10}K_b + n \log_{10}[Cu^{2+}]$ for describing the binding process. At 288 K, the slope corresponded to a binding stoichiometry of n = 0.96 ± 0.04 ≈ 1, while the intercept yielded an association constant of $K_b = (2.64 \pm 0.15) \times 10^3$ M^{-1}. At 298 K, the values were n = 1.04 ± 0.10 ≈ 1 and $K_b = (1.68 \pm 0.54) \times 10^3$ M^{-1}. At 308 K, the stoichiometry remained close to unity (n = 1.03 ± 0.09 ≈ 1), and K_b was $(2.20 \pm 0.26) \times 10^3$ M^{-1}. The consistent stoichiometry values (n ≈ 1) across all temperatures indicate formation of a 1:1 complex between the copper ion and the enzyme molecule, consistent with the presence of a single high-affinity Cu^{2+} binding site in the bCA II structure. The observed temperature dependence of K_b – a decrease at 298 K followed by partial recovery at 308 K – reflects the complex nature of thermodynamic interactions within the system. Since the static quenching mechanism was unequivocally confirmed (paragraph 2) and quantitative

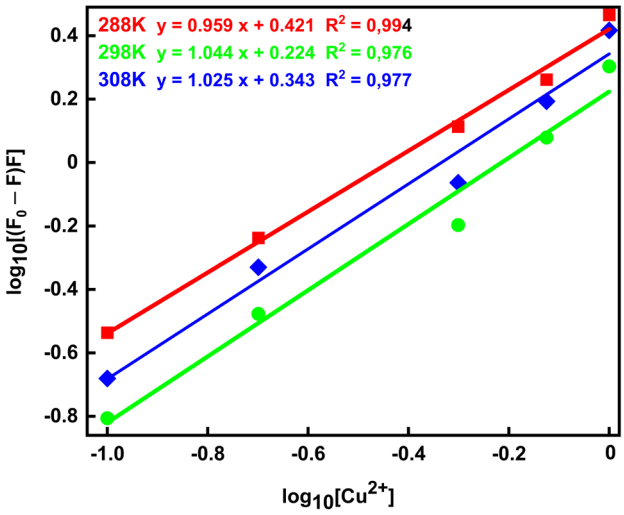

Fig. 3. Modified Stern–Volmer (double-logarithmic) plots of $\log_{10}[(F_0 – F)/F]$ *vs*. $\log_{10}[Cu^{2+}]$ for bCA II (1 µM) in 50 mM Tris buffer, pH 7.5, at 288 K (*red line and equation*), 298 K (*green line and equation*), and 308 K (*blue line and equation*). Linear fits correspond to the equation $\log_{10}[(F_0 – F)/F] = \log_{10}K_b + n \log_{10}[Cu^{2+}]$, where the slope gives the binding stoichiometry (n) and the intercept yields the association constant (K_b). Values of n, K_b, and correlation coefficients (R^2) are summarized in Table 2.

binding parameters (K_b and n) were reliably determined at three temperatures, it is now feasible to proceed to thermodynamic analysis of the interaction. This requires application of the van't Hoff equation by plotting $\ln K_b$ *vs*. 1/T, enabling calculation of standard thermodynamic parameters: the Gibbs free energy change (ΔG°), enthalpy

change (ΔH°), and entropy change (ΔS°) of binding. The signs and magnitudes of ΔH° and ΔS° will allow identification of the dominant intermolecular forces – electrostatic interactions, hydrophobic effects, hydrogen bonding, or van der Waals forces – governing Cu^{2+} affinity for the active site or an allosteric site of carbonic anhydrase II.

Thermodynamic characterization of Cu^{2+} bCA II: Thermodynamic analysis of Cu^{2+} binding to bCA II was performed to elucidate the physicochemical forces governing the interaction. The Gibbs free energy change (ΔG°) was calculated directly from the temperature-dependent association constants (K_b) using the relationship $\Delta G° = -RT \ln K_b$, with error propagation applied as $\sigma\Delta G = RT (\sigma K_b/K_b)$. This yielded ΔG° values of –18.86 ± 0.14 kJ mol^{-1} (288 K), –18.40 ± 0.80 kJ mol^{-1} (298 K), and –19.71 ± 0.30 kJ mol^{-1} (308 K). The negative ΔG° values across all temperatures confirm spontaneous binding, with minimal affinity observed at physiological temperature (298 K) and unexpectedly strengthened binding at 308 K.

To determine the enthalpic (ΔH°) and entropic (ΔS°) contributions, the van't Hoff analysis was conducted by plotting $\ln K_b$ *vs.* 1/T (Fig. 4, Table 3). Critical assessment of the data revealed non-linearity across the full 288–308 K range: K_b decreased from 2.64 × 10^3 M^{-1} (288 K) to 1.68 × 10^3 M^{-1} (298 K), consistent with exothermic binding, but increased to 2.20 × 10^3 M^{-1} at 308 K – contradicting the expected temperature dependence for a single thermodynamic mechanism. Pairwise calculations confirmed this transition: the 288 → 298 K interval yielded ΔH° = –32.3 ± 23.3 kJ mol^{-1} (exothermic), whereas the 298 → 308 K interval gave ΔH° = +20.6 ± 15.7 kJ mol^{-1} (endothermic). This sign inversion indicates a temperature-dependent shift in the dominant binding forces, likely associated with protein conformational changes – a pattern consistent with previous findings for bovine serum albumin (Bai *et al.* 2023). Consequently, linear van't Hoff analysis was restricted to the 288–298 K range, where ΔH° = –32.3 ± 23.3 kJ mol^{-1} and ΔS° = –46.5 ± 80.9 J mol^{-1} K^{-1} were obtained. The large relative error in ΔS° (exceeding its magnitude) precludes statistically significant interpretation of the entropy term; however, the negative ΔH° – despite its substantial uncertainty – indicates that binding in this temperature range is enthalpically driven, characteristic of specific interactions such as coordination bonds and hydrogen bonding within the active site.

The anomalous affinity increase at 308 K, coupled with the transition to endothermic behavior, suggests a mechanistic shift potentially involving partial structural rearrangement of bCA II. This may entail weakening of specific coordination interactions alongside enhanced hydrophobic effects or release of ordered water molecules, leading to the formation of less specific but thermodynamically stabilized complexes. The consistently negative ΔG° values confirm that Cu^{2+} binding remains spontaneous across the entire temperature range, while the complex enthalpy–entropy compensation pattern reflects the dual nature of metalloprotein–metal ion interactions, where both coordination chemistry and solvent reorganization modulate affinity in a temperature-sensitive manner.

Justification for the applicability of bCA II data to plant carbonic anhydrases: Despite structural and mechanistic differences between mammalian α-carbonic anhydrase (CA), such as bCA II (where Zn^{2+} is coordinated by three His residues and H_2O/OH^-), and plant CAs (encompassing α-, β-, and γ-classes, with β-CAs predominant and

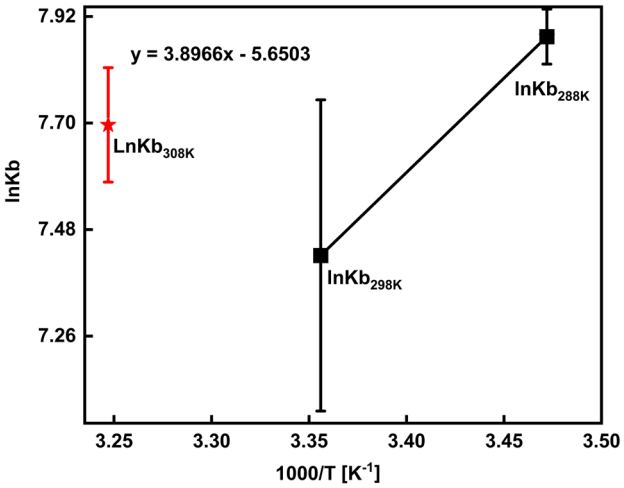

Fig. 4. Van't Hoff plot of $\ln K_b$ *vs.* $10^3/T$ [K^{-1}] for Cu^{2+} binding to bCA II (1 μM) in 50 mM Tris buffer, pH 7.5. The linear fit (*solid line*) corresponds to the equation $\ln K_b = -\Delta H°/R \times (1/T) + \Delta S°/R$, where the slope and intercept yield the thermodynamic parameters ΔH° and ΔS°, respectively. Thermodynamic parameters (ΔH°, ΔS°, at 298 K) derived from the fit are summarized in Table 3.

Table 3. Thermodynamic parameters for Cu^{2+} binding to bCA II derived from van't Hoff analysis (Fig. 4). Standard Gibbs free energy changes (ΔG°) were calculated directly at each experimental temperature using ΔG° = –R × T × lnKb. Enthalpy changes (ΔH°), and entropy changes (ΔS°) were obtained from the slope and intercept of the linear van't Hoff plot (lnKb *vs.* 1/T) over specified temperature intervals. Values are expressed as mean ± 95% confidence interval (CI) where applicable. Negative ΔG° values indicate spontaneous binding; the sign of ΔH° distinguishes exothermic (negative) from endothermic (positive) processes. All measurements were performed in 50 mM Tris buffer, pH 7.5.

pH	T [K]	ΔG°, [kJ mol^{-1}]	ΔH°, [kJ mol^{-1}]	Process	ΔS°, [J × mol^{-1} K^{-1}]
7.5	288	−18.86 ± 0.14	288–298 K: ΔH = –32.3 ± 23.3	exothermic	–46.5 ± 80.9
	298	−18.40 ± 0.80			
	308	−19.71 ± 0.30	298–308 K: ΔH = +20.6 ± 15.7	endothermic	

featuring Zn^{2+} coordinated by two Cys, one His, and one Asp, while γ-CAs may utilize Fe^{2+} or Zn^{2+}), data on Cu^{2+} effects from bCA II apply to plant CAs due to the conserved reliance on a metal ion (primarily Zn^{2+}) for catalyzing CO_2 hydration, where Cu^{2+} inhibits similarly by substituting Zn^{2+} or coordinating to it, disrupting the nucleophilic attack of OH^- on CO_2. All CA classes exhibit convergent evolution in their mechanism: the metal lowers the pKa of water to ~7.0, generating OH^- for CO_2 attack followed by proton transfer, rendering the active site vulnerable to metal substitution by Cu^{2+} regardless of ligands. In bCA II, Cu^{2+} replaces Zn^{2+}, altering geometry to trigonal-bipyramidal and impairing the proton shuttle *via* His_{64}, akin to plant β-CAs, where Cu^{2+} binds Cys/His residues, blocking the active site. Structural variations (*e.g.*, Cys in β-CAs *vs*. His in α) affect affinity but not the core principle, as Cu^{2+} forms stable complexes with these residues, displacing Zn^{2+} across domains of life (Lionetto *et al.* 2016, Supuran 2016b, Jonsson and Liljas 2020, Kircheva *et al.* 2024). Metal inhibition, including by Cu^{2+}, follows common modes such as Zn^{2+} binding (tetrahedral or trigonal-bipyramidal), anchoring to Zn-bound water, or site occlusion, applicable to α-, β-, and γ-CAs. In bCA II, Cu^{2+} targets His64 or replaces Zn^{2+}, mirroring β-CAs from algae like *Coccomyxa*, where metals block the site despite Cys coordination, with Cu^{2+} affinity preserved. This yields comparable IC_{50} values in the micromolar range across classes. For γ-CAs, Cu^{2+} inhibits *via* His coordination (Ladner *et al.* 2007, Huang *et al.* 2011, Lionetto *et al.* 2016, Supuran 2016b, Di Fiore *et al.* 2022). Direct evidence from plant β-CAs shows Cu^{2+} inhibition by Zn^{2+} substitution or His/Cys binding, leading to catalytic loss, as in *E. coli* β-CA models (Ki ~10–100 μM, similar to mammalian α-CAs). In *Arabidopsis*, Zn^{2+} deficiency heightens Cu^{2+} sensitivity, disrupting CO_2 assimilation akin to bCA II. Comparative studies confirm heavy metals like Cu^{2+} inhibit mammalian α-CAs and plant/bacterial β-CAs similarly (IC_{50} 1–10 μM), despite ligand differences. In bacterial γ-CA models, Cu^{2+} alters geometry as in α-CAs (Demirdağ *et al.* 2013, Malasarn *et al.* 2013, DiMario *et al.* 2017, Del Prete *et al.* 2020, Di Fiore *et al.* 2022). Although coordination differences (*e.g.*, stronger Cys–Cu^{2+} bonds in β-CAs due to sulfur softness) may enhance inhibition compared to α-CAs, the overall outcome – catalytic suppression – remains conserved, with Cu^{2+} inducing trigonal-bipyramidal shifts and water addition in both. Crystallographic data reveal inhibitors, including metals, occlude sites similarly, with shared hydrophobic CO_2 pockets. Cu^{2+} also affects secondary sites (*e.g.*, T-2 in α-CAs) *via* His coordination in plant CAs (Huang *et al.* 2011, Frost 2014, Lionetto *et al.* 2016, Supuran 2016b, Angeli *et al.* 2020, Kim and Jo 2022). Thus, bCA II data extrapolate to plant CAs, with affinity adjustments possible. In conclusion, based on the aforementioned considerations, it is evident that data obtained from bCA II are fully applicable to other carbonic anhydrases, including plant carbonic anhydrases.

Brief review of crystallographic studies on metal binding to carbonic anhydrases (CA II): Crystallographic studies of metal binding in human carbonic anhydrase II (CA II) have revealed that the native zinc ion is tetrahedrally coordinated by three histidine residues (His94, His96, His119) and a water/hydroxide molecule, enabling ~100% catalytic activity for CO_2 hydration. Substitution with other metals alters the coordination geometry and drastically reduces activity: Co^{2+} often retains tetrahedral coordination (with pH-dependent transitions toward penta- or octahedral states; activity ≈ 50%), Ni^{2+} adopts octahedral geometry with additional water ligands (activity ≈ 2%), and Cu^{2+} exhibits trigonal-bipyramidal (penta-coordinate) coordination, correlating with near-complete loss of catalytic efficacy (activity ≈ 0%). These structural insights, including intermediate states under CO_2 pressure, anion complexes (*e.g.*, HS^-, NO_3^-), and inhibitor bindings, are detailed in key publications such as Håkansson *et al.* (1992, 1994), Mangani and Håkansson (1992), Avvaru *et al*. (2010), Song *et al.* (2012), Lomelino *et al*. (2018) (review), Kim *et al*. (2020), Andring *et al*. (2021) and others.

Conclusion: This study comprehensively characterized the interaction between Cu^{2+} ions and bCA II using steady-state fluorescence spectroscopy combined with thermodynamic analysis. Cu^{2+} induced concentration-dependent quenching of intrinsic tryptophan fluorescence without shifting the emission maximum (λ_{max} = 343 nm), indicating that the ion binds to the protein without perturbing the local environment of fluorophores or inducing global conformational changes within the studied concentration range (0–1.00 mM). Stern–Volmer analysis revealed linear F_0/F *vs*. $[Cu^{2+}]$ dependencies with K_{SV} values of $(2.75 \pm 0.17) \times 10^3$, $(1.88 \pm 0.19) \times 10^3$, and $(2.44 \pm 0.24) \times 10^3$ M^{-1} at 288 K, 298 K, and 308 K, respectively. The decrease in K_{SV} with rising temperature (288 K → 298 K), coupled with calculated quenching rate constants ($kq > 10^{11}$ M^{-1} s^{-1}) exceeding the diffusion limit, unequivocally established a static quenching mechanism mediated by ground-state complex formation. Modified Stern–Volmer analysis further demonstrated 1:1 binding stoichiometry (n ≈ 1) at all temperatures with moderate affinity constants ($K_b \approx 10^3$ M^{-1}), consistent with Cu^{2+} occupying a single specific site – likely the catalytic Zn^{2+} pocket or a proximal histidine-rich region. Thermodynamic profiling *via* van't Hoff analysis revealed spontaneous binding ($\Delta G° < 0$) across 288–308 K, with a notable temperature-dependent inversion in the enthalpy signature: exothermic binding ($\Delta H° = -32.3$ kJ mol^{-1}) dominated at lower temperatures (288–298 K), while endothermic contributions ($\Delta H° = +20.6$ kJ mol^{-1}) emerged at higher temperatures (298–308 K). This enthalpy–entropy compensation behavior suggests a dual contribution of forces: at physiological temperatures, Cu^{2+} binding is primarily driven by favorable enthalpic interactions (coordination bonds with imidazole nitrogens of active-site histidines), whereas elevated temperatures enhance the entropic component, possibly through displacement of ordered water molecules from the metal-binding pocket. Collectively, these findings demonstrate that Cu^{2+} – within the concentration range studied – binds

specifically and reversibly to bCA II with moderate affinity without denaturing the protein.

We anticipate that the information obtained will be valuable for research into the CA-like activity of extrinsic water-soluble PSII proteins and the PSII core, enriching our knowledge of metal interactions with carbonic anhydrases in plants. Furthermore, this study demonstrates how this method can be successfully employed to investigate metal–CA interactions. Overall, these results highlight the multitarget impact of copper ions and Cu^{2+}-based complexes on photosynthesis and CA activity, emphasizing that inhibition of CA activity is one of the key factors in modulating plant responses to abiotic stresses.

References

Abdulmajeed A.T.A., Gokoglan H., Ozdogru E. *et al.*: Utilizing bovine carbonic anhydrase II for enzyme-induced carbonate precipitation (EICP) in recycled concrete aggregate. – Environ. Res. **284**: 122255, 2025.

Afrin R., Alam M.T., Ikai A.: Pretransition and progressive softening of bovine carbonic anhydrase II as probed by single molecule atomic force microscopy. – Protein Sci. **14**: 1447-1457, 2005.

Andring J.T., Kim C.U., McKenna R.: Structure and mechanism of copper–carbonic anhydrase II: a nitrite reductase. Corrigendum. – IUCrJ **8**: 329, 2021.

Angeli A., Carta F., Supuran C.T.: Carbonic anhydrases: versatile and useful biocatalysts in chemistry and biochemistry. – Catalysts **10**: 1008, 2020.

Asadi V., Kardanpour R., Tangestaninejad S. *et al.*: Novel bovine carbonic anhydrase encapsulated in a metal–organic framework: a new platform for biomimetic sequestration of CO_2. – RSC Adv. **9**: 28460-28469, 2019.

Avvaru B.S., Arenas D.J., Tu C. *et al.*: Comparison of solution and crystal properties of Co(II)-substituted human carbonic anhydrase II. – Arch. Biochem. Biophys. **502**: 53-59, 2010.

Bai J., Sun X., Geng B., Ma X.: Interaction mechanism of Cu^{+}/Cu^{2+} on bovine serum albumin: vitro simulation experiments by spectroscopic methods. – Spectrochim. Acta. A **293**: 122491, 2023.

Benlloch R., Shevela D., Hainzl T. *et al.*: Crystal structure and functional characterization of photosystem II-associated carbonic anhydrase CAH3 in *Chlamydomonas reinhardtii*. – Plant Physiol. **167**: 950-962, 2015.

Burda K., Kruk J., Schmid G.H., Strzalka K.: Inhibition of oxygen evolution in Photosystem II by Cu(II) ions is associated with oxidation of cytochrome b_{559}. – Biochem. J. **371**: 597-601, 2003.

Burda K., Kruk J., Strzalka K., Schmid G.H.: Stimulation of oxygen evolution in photosystem II by copper(II) ions. – Z. Naturforsch. C **57**: 853-857, 2002.

Burda K., Kruk J., Strzałka K. *et al.*: Mössbauer studies of Cu(II) ions interaction with the non-heme iron and cytochrome b_{559} in a *Chlamydomonas reinhardtii* PSI minus mutant. – Acta Phys. Pol. A **109**: 237-247, 2006.

Del Prete S., De Luca V., Nocentini A. *et al.*: Anion inhibition studies of the beta-carbonic anhydrase from *Escherichia coli*. – Molecules **25**: 2564, 2020.

Demirdağ R., Yerlikaya E., Şentürk M. *et al.*: Heavy metal ion inhibition studies of human, sheep and fish α-carbonic anhydrases. – J. Enzym. Inhib. Med. Chem. **28**: 278-282, 2013.

Di Fiore A., De Luca V., Langella E. *et al.*: Biochemical, structural, and computational studies of a γ-carbonic anhydrase from the pathogenic bacterium *Burkholderia pseudomallei*. – Comput. Struct. Biotechnol. J. **20**: 4185-4194, 2022.

DiMario R.J., Clayton H., Mukherjee A. *et al.*: Plant carbonic anhydrases: structures, locations, evolution, and physiological roles. – Mol. Plant **10**: 30-46, 2017.

Fedai M., Shen J., Bognár Z. *et al.*: Advances in biomimetic carbonic anhydrase strategies for CO_2 capture. – Trends Biotechnol. **43**: 3040-3055, 2025.

Finazzi Agrò A., Morpurgo L., Mondovi B.: Effect of metal binding on the intrinsic fluorescence of bovine carbonic anhydrase. – Biophys. Chem. **2**: 151-157, 1974.

Frost S.C.: Physiological functions of the alpha class of carbonic anhydrases. – In: Frost S.C., McKenna, R. (ed.): Carbonic Anhydrase: Mechanism, Regulation, Links to Disease, and Industrial Applications. Subcellular Biochemistry. Vol. 75. Pp. 9-30. Springer, Dordrecht 2014.

Gitlin I., Gudiksen K.L., Whitesides G.M.: Effects of surface charge on denaturation of bovine carbonic anhydrase. – ChemBioChem **7**: 1241-1250, 2006.

Håkansson K., Carlsson M., Svensson L.A., Liljas A.: Structure of native and apo carbonic anhydrase II and structure of some of its anion-ligand complexes. – J. Mol. Biol. **227**: 1192-1204, 1992.

Håkansson K., Wehnert A., Liljas A.: X-ray analysis of metal-substituted human carbonic anhydrase II derivatives. – Acta Crystallogr. D **50**: 93-100, 1994.

Huang S., Hainzl T., Grundström C. *et al.*: Structural studies of β-carbonic anhydrase from the green alga *Coccomyxa*: inhibitor complexes with anions and acetazolamide. – PLoS ONE **6**: e28458, 2011.

Jonsson B.-H., Liljas A.: Perspectives on the classical enzyme carbonic anhydrase and the search for inhibitors. – Biophys. J. **119**: 1275-1280, 2020.

Karacan M.S., Rodionova M.V., Tunç T. *et al.*: Characterization of nineteen antimony(III) complexes as potent inhibitors of photosystem II, carbonic anhydrase, and glutathione reductase. – Photosynth. Res. **130**: 167-182, 2016.

Karacan M.S., Zharmukhamedov S.K., Mamaş S. *et al.*: Screening of novel chemical compounds as possible inhibitors of carbonic anhydrase and photosynthetic activity of photosystem II. – J. Photoch. Photobio. B **137**: 156-167, 2014.

Kim J.H., Jo B.H.: A colorimetric CO_2 hydration assay for facile, accurate, and precise determination of carbonic anhydrase activity. – Catalysts **12**: 1391, 2022.

Kim J.K., Lee C., Lim S.W. *et al.*: Elucidating the role of metal ions in carbonic anhydrase catalysis. – Nat. Commun. **11**: 4557, 2020.

Kircheva N., Angelova S., Dudev T.: Carbonic anhydrases: different active sites, same metal selectivity rules. – Molecules **29**: 1995, 2024.

Kose L.P., Gülçin İ., Özdemir H. *et al.*: The effects of some avermectins on bovine carbonic anhydrase enzyme. – J. Enzym. Inhib. Med. Chem. **31**: 773-778, 2016.

Krishnamurthy V.M., Kaufman G.K., Urbach A.R. *et al.*: Carbonic anhydrase as a model for biophysical and physical-organic studies of proteins and protein–ligand binding. – Chem. Rev. **108**: 946-1051, 2008.

Kupriyanova E., Pronina N., Los D.: Carbonic anhydrase – a universal enzyme of the carbon-based life. – Photosynthetica **55**: 3-19, 2017.

Ladner C.L., Turner R.J., Edwards R.A.: Development of indole chemistry to label tryptophan residues in protein for determination of tryptophan surface accessibility. – Protein Sci. **16**: 1204-1213, 2007.

Lakkis M.M., Bergenhem N.C.H., Tashian R.E.: Expression of

mouse carbonic anhydrase VII in *E. coli* and demonstration of its CO_2 hydrase activity. – Biochem. Bioph. Res. Co. **226**: 268-272, 1996.

Lakowicz J.R.: Principles of Fluorescence Spectroscopy. Pp. 954. Springer, New York 2006.

Lee C.H., Jang E.K., Yeon Y.J., Pack S.P.: Stabilization of bovine carbonic anhydrase II through rational site-specific immobilization. – Biochem. Eng. J. **138**: 29-36, 2018.

Lionetto M.G., Caricato R., Giordano M.E., Schettino T.: The complex relationship between metals and carbonic anhydrase: new insights and perspectives. – Int. J. Mol. Sci. **17**: 127, 2016.

Lomelino C.L., Andring J.T., McKenna R.: Crystallography and its impact on carbonic anhydrase research. – Int. J. Med. Chem. **2018**: 9419521, 2018.

Malasarn D., Kropat J., Hsieh S.I. *et al.*: Zinc deficiency impacts CO_2 assimilation and disrupts copper homeostasis in *Chlamydomonas reinhardtii*. – J. Biol. Chem. **288**: 10672-10683, 2013.

Mangani S., Håkansson K.: Crystallographic studies of the binding of protonated and unprotonated inhibitors to carbonic anhydrase using hydrogen sulphide and nitrate anions. – Eur. J. Biochem. **210**: 867-871, 1992.

McConnell I.L., Badger M.R., Wydrzynski T., Hillier W.: A quantitative assessment of the carbonic anhydrase activity in photosystem II. – BBA-Bioenergetics **1767**: 639-647, 2007.

Mourad A.A.H., Mohammad A.F., Al-Marzouqi A.H.: Evaluation of bovine carbonic anhydrase for promoting CO_2 capture *via* reaction with KOH and high-salinity reject brine. – J. CO_2 Util. **81**: 102714, 2024.

Nemtseva E.V., Lashchuk O.O., Gerasimova M.A. *et al.*: Fluorescence lifetime components reveal kinetic intermediate states upon equilibrium denaturation of carbonic anhydrase II. – Methods Appl. Fluoresc. **6**: 015006, 2017.

Nocentini A., Supuran C.T., Capasso C.: An overview on the recently discovered iota-carbonic anhydrases. – J. Enzym. Inhib. Med. Chem. **36**: 1988-1995, 2021.

Phan D.T., Burns R.C., Puxty G. *et al.*: A study of bovine and human carbonic anhydrases as a model enzyme system for CO_2 hydration in post combustion capture. – Int. J. Greenh. Gas Control **37**: 85-89, 2015.

Rajaraman K., Raman B., Rao C.M.: Molten-globule state of carbonic anhydrase binds to the chaperone-like α-crystallin. – J. Biol. Chem. **271**: 27595-27600, 1996.

Rodionova M.V., Zharmukhamedov S.K., Karacan M.S. *et al.*: Evaluation of new Cu(II) complexes as a novel class of inhibitors against plant carbonic anhydrase, glutathione reductase, and photosynthetic activity in photosystem II. – Photosynth. Res. **133**: 139-153, 2017.

Rudenko N.N., Ignatova L.K., Fedorchuk T.P., Ivanov B.N.: Carbonic anhydrases in photosynthetic cells of higher plants. – Biochemistry-Moscow **80**: 674-687, 2015.

Saito R., Sato T., Ikai A., Tanaka N.: Structure of bovine carbonic anhydrase II at 1.95 Å resolution. – Acta Crystallogr. D **60**: 792-795, 2004.

Sargolzaei J., Jalali E., Rajabi P.: Insights into the binding of buspirone to human serum albumin using multi-spectroscopic and molecular docking techniques. – Heliyon **10**: e29430, 2024.

Sarraf N.S., Saboury A.A., Ranjbar B., Moosavi-Movahedi A.A.: Structural and functional changes of bovine carbonic anhydrase as a consequence of temperature. – Acta Biochim. Pol. **51**: 665-671, 2004.

Sciaky M., Limozin N., Filippi-Foveau D. *et al.*: [Primary structure of bovine erythrocyte carbonic anhydrase CI: II. – Complete sequence.] – Biochimie **58**: 1071-1082, 1976. [In French]

Shitov A.V., Pobeguts O.V., Smolova T.N. *et al.*: Manganese-dependent carboanhydrase activity of photosystem II proteins. – Biochemistry-Moscow **74**: 509-517, 2009.

Shitov A.V., Terentyev V.V., Govindjee G.: High and unique carbonic anhydrase activity of Photosystem II from *Pisum sativum*: Measurements by a new and very sensitive fluorescence method. – Plant Physiol. Biochem. **221**: 109516, 2025.

Shutova T., Kenneweg H., Buchta J. *et al.*: The photosystem II-associated Cah3 in *Chlamydomonas* enhances the O_2 evolution rate by proton removal. – EMBO J. **27**: 782-791, 2008.

Song H., Wilson D.L., Farquhar E.R. *et al.*: Revisiting zinc coordination in human carbonic anhydrase II. – Inorg. Chem. **51**: 11098-11105, 2012.

Stein P.J., Henkens R.W.: Detection of intermediates in protein folding of carbonic anhydrase with fluorescence emission and polarization. – J. Biol. Chem. **253**: 8016-8018, 1978.

Supuran C.T.: Carbonic anhydrases: novel therapeutic applications for inhibitors and activators. – Nat. Rev. Drug Discov. **7**: 168-181, 2008.

Supuran C.T.: Structure and function of carbonic anhydrases. – Biochem. J. **473**: 2023-2032, 2016a.

Supuran C.T.: How many carbonic anhydrase inhibition mechanisms exist? – J. Enzym. Inhib. Med. Chem. **31**: 345-360, 2016b.

Supuran C.T.: Carbonic anhydrase versatility: from pH regulation to CO_2 sensing and metabolism. – Front. Mol. Biosci. **10**: 1326633, 2023.

Tiwari A., Kumar P., Singh S., Ansari S.A.: Carbonic anhydrase in relation to higher plants. – Photosynthetica **43**: 1-11, 2005.

Tobolovskaya Y., Medvedev J.J., Medvedeva X.V. *et al.*: The bovine carbonic anhydrase promoted dehydration of bicarbonate to CO_2 for the electrochemical production of syngas. – J. CO_2 Util. **71**: 102461, 2023.

Wani T., Bakheit A.H., Al-Majed A.-R.A. *et al.*: Study of the interactions of bovine serum albumin with the new anti-inflammatory agent 4-(1,3-dioxo-1,3-dihydro-2H-isoindol-2-yl)-N'-[(4-ethoxy-phenyl)methylidene]benzohydrazide using a multi-spectroscopic approach and molecular docking. – Molecules **22**: 1258, 2017.

Wei X., Ding S., Jiang Y. *et al.*: Conformational changes and inactivation of bovine carbonic anhydrase II in 2,2,2-trifluoroethanol solutions. – Biochemistry-Moscow **71**: S77-S82, 2006.

Yruela I.: Copper in plants. – Braz. J. Plant Physiol. **17**: 145-156, 2005.

Zharmukhamedov S.K., Shabanova M.S., Huseynova I.M. *et al.*: Probing the influence of novel organometallic copper(II) complexes on spinach PSII photochemistry using OJIP fluorescence transient measurements. – Biomolecules **13**: 1058, 2023.

Zharmukhamedov S.K., Shabanova M.S., Rodionova M.V. *et al.*: Effects of novel photosynthetic inhibitor $[CuL_2]Br_2$ complex on Photosystem II activity in spinach. – Cells **11**: 2680, 2022.